

# Role of Solidification in Submerged Entry Nozzle Clogging During Continuous Casting of Steel

Hadi Barati, Menghuai Wu,\* Abdellah Kharicha, and Andreas Ludwig

Metallurgists are embroiled in a debate on the role of solidification in submerged entry nozzle (SEN) clogging during continuous casting of steel: does clogging originate from solidification, or does clogging cause the solidification? This study tries to clarify this debate. An enthalpy-based mixture continuum model is used to simulate solidification in a clog structure. The 3D structure of the clog is reconstructed using X-ray tomography images of an as-clogged piece in an SEN, and is directly used in the numerical model. The flow and solidification in the open pores/channels of the clog structure are then calculated. The modeling results demonstrate that although solidification does occur deep in the clog structure as the melt flow is stopped, a gap remains between the solidification and clog fronts. This gap signifies an open-channel clog region, and the clog structure in this region needs to be mechanically strong to withstand the impact of the melt flow; otherwise, fragmentation occurs. The study verifies that the solidification cannot occur before clogging if the molten steel has sufficient superheat and the SEN is properly preheated. A SEN made of an isolating refractory material can postpone the clogging, thereby extending its service life.

Great research efforts have been undertaken to understand and control the clogging. The following mechanisms have been proposed as the reason for clogging: 1) transport/deposit of nonmetallic inclusions (NMIs), i.e., deoxidation and reoxidation products, from the molten steel to/on the SEN wall;<sup>[1–3]</sup> 2) thermochemical reactions between the refractory and the melt at the SEN wall;<sup>[4,5]</sup> 3) oxidation of steel attributed to the oxygen being sucked through the porous refractory wall because of a negative operational pressure in the SEN;<sup>[6]</sup> 4) endogenous precipitation of alumina from the steel due to the reduced solubility of oxygen at lower temperatures near the SEN wall;<sup>[7,8]</sup> and 5) solidification of the steel on the SEN wall.<sup>[9,10]</sup> Although increasing recent evidence has suggested that the deposition of NMIs on the SEN wall is the primary cause of the clogging,<sup>[11–14]</sup> one still cannot rule out the other mechanisms. For example, the metallographic

## 1. Introduction


A submerged entry nozzle (SEN), a tube-shaped device composed of refractory, is used to conduct molten steel from the tundish to the mold during continuous casting of steel. During the process, the SEN serves to protect the melt from oxidation and to stabilize the casting process. However, a gradual build-up of solid materials on the inner wall of the SEN may lead to so-called clogging, which can seriously deteriorate the steel quality, and even cause a disruption in the operation.

analyses of as-clogged SEN samples exhibited approximately 50 vol% of frozen steel in the clog material,<sup>[15,16]</sup> which raises a question regarding the role of solidification in the clogging: does clogging originate from solidification, or does the clogging cause the solidification? In a previous study, the current authors discovered that molten steel with superheat of 10–20 K and flowing with a velocity of approximately 1 m s<sup>−1</sup> through a preheated SEN would never solidify.<sup>[17]</sup> Most probably, the solidification occurs in conjunction with other mechanisms, e.g., as-captured steel in the porous region of a clog network may also be prone to solidification.

The objective of this study was to comprehensively study the possibility of solidification and its role in clogging of an engineering-scale SEN. A transient clogging model has already been developed for this purpose<sup>[18,19]</sup> and evaluated against a laboratory experiment (clogging simulator).<sup>[15]</sup> The model simulated the mechanism of NMI transport/deposition on the nozzle wall. The clog was treated as a porous network constructed from as-deposited NMI particles. However, the morphology of the porous network cannot be modeled, and must be set as a model input. The clog morphology can be described using three parameters: the diameter of alumina particles ( $d_p$ ), the average volume fraction of the particles ( $\bar{f}_p$ ), and the diameter of large pores ( $D_{pore}$ ), all of which have to be determined through a post-mortem analysis of the as-clogged nozzle. Therefore, an alternative modeling approach was taken in the current study. The 3D structure of a clog, obtained by performing X-ray tomography on an as-clogged SEN, was constructed and directly utilized in the model. Instead

Dr. H. Barati  
K1-MET  
Franz-Josef Street 18, 8700 Leoben, Austria

Dr. H. Barati, Prof. M. Wu, Prof. A. Kharicha, Prof. A. Ludwig  
Chair for Modeling and Simulation of Metallurgical Processes,  
Department of Metallurgy  
Montanuniversitaet  
Franz-Josef Street 18, 8700 Leoben, Austria  
E-mail: menghuai.wu@unileoben.ac.at

 The ORCID identification number(s) for the author(s) of this article can be found under <https://doi.org/10.1002/srin.202000230>.

© 2020 The Authors. Published by WILEY-VCH Verlag GmbH & Co. KGaA, Weinheim. This is an open access article under the terms of the Creative Commons Attribution License, which permits use, distribution and reproduction in any medium, provided the original work is properly cited.

DOI: 10.1002/srin.202000230

of tracking the clog growth dynamically, the clog was assumed to follow a step-wise growth pattern with a predefined procedure and morphology, so that the melt solidification in the channels of the porous network, in response to the progress of the clog front and the different cooling conditions in the SEN, can be investigated with high resolution.

## 2. Modeling

### 2.1. Description

As shown in **Figure 1a**, the 3D structure of an as-clogged piece in an SEN, formed during continuous casting of ultra-low carbon steel, was obtained with X-ray tomography. The clog was composed of alumina and other nonmetallic phases, which formed a porous network with open pores/channels, a majority of which were connected to each other. The porous region of the clog can be assumed to be filled with steel, either in the liquid or solid state, during the clogging process. The minimum open pore/channel size was approximately 0.19 mm and the average size of the open pores was roughly 1.2 mm. However, the X-ray tomography resolution could not sufficiently capture the structural details inside the clog, e.g., nonmetallic particles that help in the buildup of the clog at a scale of a few  $\mu\text{m}$ . A representative segment ( $6 \times 6 \times 6 \text{ mm}^3$ ) of the clog structure, extracted from the X-ray tomography results, was utilized in the flow and solidification model.

As shown in **Figure 1b**, the calculation of the whole SEN is not feasible, because an extremely fine mesh, of the order of 0.1 mm, is required to resolve the flow and the thermal field inner porous region of the clog. In a practical scenario, the inner diameter of the SEN would be  $\phi 70 \text{ mm}$ . As a result, the whole SEN, with a diameter of 70 mm and a height of 420 mm, assuming a clog thickness of 6 mm, would require  $\approx 165$  million computational cells. Therefore, only a sector of the SEN, measuring  $10^\circ$ , was simulated in this study (**Figure 1b**). The global flow and solidification pattern in the SEN was assumed to be quasi axis-symmetrical. The considered SEN height (420 mm) was partitioned into 35 sections. The calculation starts from section 1.

The converged calculation result on the bottom surface (outlet) of each section was set as the inlet (top surface) boundary condition for the next section. Each section height was set as 12 mm, which is two times the height of the extracted clog segment (**Figure 1a**). Therefore, the extracted clog segment (6 mm) was twinned and fitted into the fluid domain (section height of 12 mm) as a part of the clog. To maintain the continuity of the flow channels in the clog passing through the section border, the structure of the clog segment was further twinned/mirrored on the horizontal plane. Similarly, the growth of the clog was also modeled by vertically mirroring the clog segment in a step-wise manner from the SEN wall in toward the center.

**Figure 2** shows the mesh in a part of the calculation domain. The different material zones are marked in different colors. A uniform hexahedron mesh was considered for the clog region, whereas a tetrahedron mesh (not shown in the figure) was considered for the SEN center. The flow and solidification calculations were performed only for regions inside the SEN, i.e., the so-called fluid domain, which includes the steel (liquid, mush, and solid) and the clog, and only heat transfer calculations were performed for the SEN wall. The computational cells in the fluid domain were initialized with liquid steel (free to flow). Additional treatment was performed for the clog cells, where the velocity was set as zero and the material properties were set same as those of the clog (alumina). It is known that liquid steel can solidify, i.e., first transform into a solid-liquid mixture (mushy zone), then into solid steel. An average mesh size of 0.12 mm was used in our study and the total number of cells in the computation domain was 828 900. The sensitivity of the calculation result to the mesh quality is discussed in Section 4.

The other model assumptions/simplifications were as follows: 1) The clog grows in a step-wise manner, and with uniform thickness from the SEN wall. 2) The clog growth is a slow process in comparison to the solidification; for a given clog thickness, a quasi-steady-state solidification profile can be achieved. 3) The clog has a rigid and stable structure, i.e., any fragmentation/detachment is ignored. 4) The SEN wall is considered as being composed of a solid material with uniform thermo-physical properties.

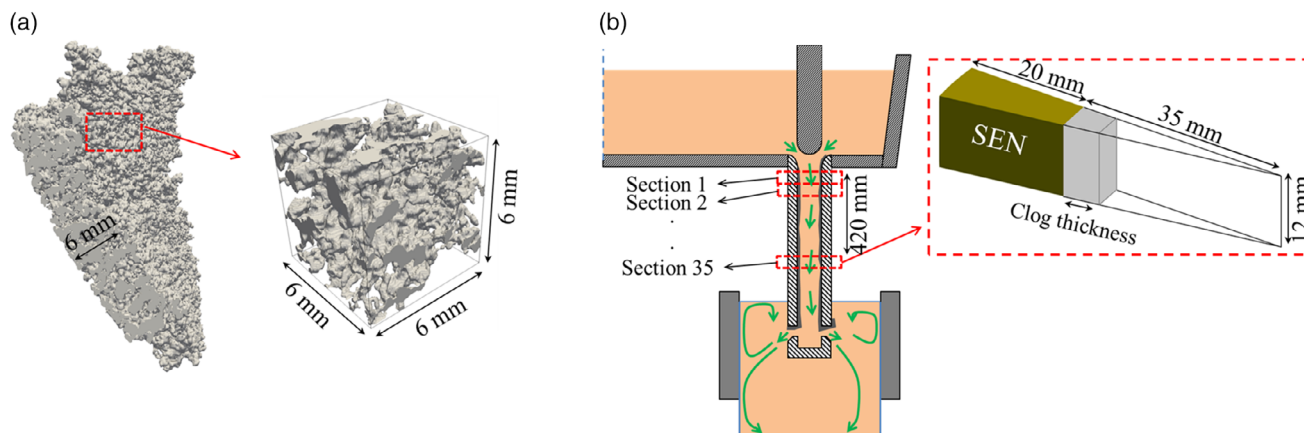


**Figure 1.** 3D reconstruction of the clog structure and configuration of the calculation domain. a) X-ray tomography image of an as-clogged piece; b) schematic of the clogging process in a SEN and the configuration and partitioning of the calculation domain.

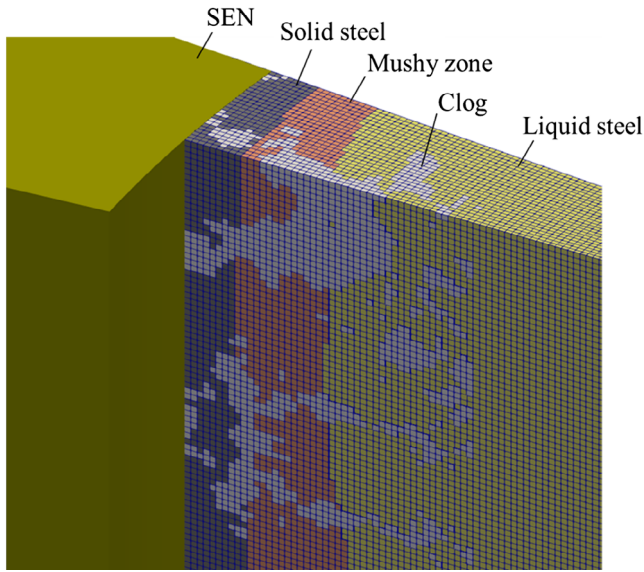


**Figure 2.** Enmeshment of the calculation domain. Only a part of the calculation domain is presented for better visualization. Material zones are marked in different colors: SEN wall in green, clog in gray, solid steel in dark gray, mushy zone in magenta, and molten steel in light green.

## 2.2. Governing Equations

The conservation equations for mass, momentum, and enthalpy are listed in **Table 1**. A shear–stress transport  $k$ – $\omega$  model was considered for the turbulence.<sup>[20]</sup> An enthalpy-based mixture continuum model was adopted for calculating the solidification by assuming the variation in the liquid volume phase ( $f_l$ ) as a linear function of the temperature.

$$f_l = \frac{(T - T_{\text{sol}})}{(T_{\text{liq}} - T_{\text{sol}})} \quad (1)$$

**Table 1.** Governing equations for fluid flow and heat transfer.

Conservation equations		Symbol definition
Mass	$\nabla \cdot (\rho \vec{u}) = 0$ (3)	$\rho$ : density [ $\text{kg m}^{-3}$ ]
Momentum	$\rho \frac{\partial \vec{u}}{\partial t} + \nabla \cdot (\rho \vec{u} \vec{u}) = -\nabla p + \nabla \cdot (\mu \nabla \vec{u}) + \vec{S}_u$ (4)	$\mu$ : viscosity [ $\text{kg m}^{-1} \text{s}^{-1}$ ]
Turbulence kinetic energy	$\rho \frac{\partial k}{\partial t} + \nabla \cdot (\rho k \vec{u}) = \nabla \cdot (\Gamma_k \nabla k) + \tilde{G}_k - Y_k + S_k$ (5)	$t$ : time [s] $\vec{u}$ : velocity [ $\text{m s}^{-1}$ ]
Specific dissipation rate	$\rho \frac{\partial \omega}{\partial t} + \nabla \cdot (\rho \omega \vec{u}) = \nabla \cdot (\Gamma_\omega \nabla \omega) + G_\omega - Y_\omega + D_\omega + S_\omega$ (6)	$k$ : turbulence kinetic energy [ $\text{m}^2 \text{s}^{-2}$ ] $\omega$ : specific dissipation rate of turbulence kinetic energy [ $\text{s}^{-1}$ ]
Enthalpy	$\frac{\partial}{\partial t} (\rho h) + \nabla \cdot (\rho \vec{u} h) = \nabla \cdot (\lambda \nabla T) + L \rho \frac{\partial f_s}{\partial t}$ (7)	$\Gamma_k, \Gamma_\omega$ : diffusivity for $k$ and $\omega$ [ $\text{kg m}^{-1} \text{s}^{-1}$ , $\text{kg m}^{-2}$ ] $\tilde{G}_k, G_\omega$ : generation of turbulence kinetic energy for $k$ and $\omega$ [ $\text{kg m}^{-1} \text{s}^{-3}$ , $\text{kg m}^{-2} \text{s}^{-2}$ ] $Y_k, Y_\omega$ : dissipation of $k$ and $\omega$ [ $\text{kg m}^{-1} \text{s}^{-3}$ , $\text{kg m}^{-2} \text{s}^{-2}$ ] $D_\omega$ : cross-diffusion term of $\omega$ [ $\text{kg m}^{-2} \text{s}^{-2}$ ] $S_k, S_\omega, \vec{S}_u$ : source terms in the mushy zone [ $\text{kg m}^{-1} \text{s}^{-3}$ , $\text{kg m}^{-2} \text{s}^{-2}$ , $\text{kg m}^{-2} \text{s}^{-2}$ ] $h$ : sensible enthalpy $T$ : temperature $\lambda$ : heat conductivity $L$ : latent heat $f_s$ : solid fraction

where  $T_{\text{liq}}$  and  $T_{\text{sol}}$  are the liquidus and solidus temperatures. The end terms of Equation (4)–(6) given in Table 1 are source terms, which are defined to mimic the damping effects of the mushy zone. They are calculated as

$$S_\phi = -\frac{(1 - f_l)^2}{(f_l)^3} \frac{\mu}{6 \times 10^{-4} (\lambda_1)^2} \phi \quad (2)$$

where  $\lambda_1$  is the primary dendrite arm spacing of the as-solidifying steel.  $\phi$  can be the velocity  $\vec{u}$ , the kinetic turbulence energy  $k$ , or its specific dissipation rate  $\omega$ .<sup>[21]</sup> If a cell is occupied by the clog,  $f_l$  in this cell is set as 0.0, which means that the cell is completely solid (same as solid steel). By setting  $f_l = 0.0$ ,  $\phi$  is forced to zero.

In the enthalpy equation (Equation (7)), the last term on the right-hand side represents the latent heat release due to solidification, where the fraction solid ( $f_s$ ) is equal to  $1 - f_l$ . This latent heat source term is only valid for the computation cells occupied by steel. For the clog-filled cells, the source term is set as 0.0. In other words, the clog is treated as “solid steel” but with different thermo-physical properties.

## 2.3. Simulation Settings

In this study, the casting of low-carbon steel was simulated. The clog material was alumina, as it is the main component found in as-clogged structures during continuous casting of low-carbon steels.<sup>[16]</sup> The properties of the different materials are listed in **Table 2**. The thermo-physical properties of alumina and the SEN refractory are quite constant across the temperature range used in normal operations. However, the density, viscosity, and thermal conductivity of the steel have to be considered as temperature-dependent, as shown in **Figure 3**. The SEN wall is usually composed of a mixture of different refractory materials. A numerical parameter study was performed by varying the thermal conductivity values according to the typical SEN refractory materials used in the industry.

**Table 2.** Thermo-Physical properties of materials.

	Steel	Alumina	SEN refractory
Density [ $\text{kg m}^{-3}$ ]	Figure 3	3700.0	2430.0
Viscosity [ $\text{Pa s}$ ]	Figure 3	–	–
Specific heat [ $\text{J kg}^{-1} \text{K}^{-1}$ ]	700.0	700.0	1416.56
Thermal conductivity [ $\text{W m}^{-1} \text{K}^{-1}$ ]	Figure 3	35.0	18.0, 11.0, 6.0
Liquidus temperature [K]	1807.0	–	–
Solidus temperature [K]	1789.0	–	–
Latent heat [ $\text{kJ kg}^{-1}$ ]	243.0	–	–

Notably, as only one set of the enthalpy equation was solved for the whole fluid domain, the numerical study was conducted using the same specific heat settings for both the clog (alumina) and steel.

For the SEN outer wall (Figure 1b), which is exposed to the atmosphere, a combined convection heat transfer and radiation boundary condition was applied. The convection heat-transfer coefficient and free-stream temperature were set as  $80 \text{ W m}^{-2} \text{K}^{-1}$  and 573 K, respectively. The radiation emissivity was 0.7.<sup>[22]</sup> It was assumed that the SEN inner wall had perfect contact with steel, i.e., there is no heat transfer resistance. The front and back faces of the calculation domain were set as symmetric planes.

During continuous casting, the melt flow rate should be kept constant to satisfy a constant casting speed, which is achieved through an adjustment of the stopper rod position or the slide gate in the SEN whenever clogging occurs. In our numerical model, the melt mass flow rate through the SEN was imposed as a constant value at  $1.58 \text{ kg s}^{-1}$ . The flow boundary for the first section inlet was set as a fully developed flow pattern with a constant mass flow rate ( $1.58 \text{ kg s}^{-1}$ ) and a constant temperature (1822 K). For the subsequent sections, the inlet boundary

conditions of the current section were defined based on the outlet data of the previous section. At the outlet of each section, a pressure-outlet boundary condition was set for the flow and a zero-gradient condition for the temperature.

The governing equations were solved using a commercial code ANSYS-FLUENT. The solidification model was extended with user-defined functions (UDFs). The computations were performed on a high-performance computer cluster with 30 CPUs (2.9 GHz), and the computation for each simulation took approximately 8 h.

### 3. Results

Similar to a previous study,<sup>[17]</sup> solidification did not occur before the clog growth in our case with a superheat of 15 K. **Figure 4a** shows the temperature profiles along the SEN radial direction during clogging, where the liquidus and solidus lines indicate the solidification mushy zone. Without clogging, the maximum temperature drop at the wall was approximately 2 K, i.e., the temperature remained approximately 13 K above the liquidus. As the clog thickness increased to 3 mm, the minimum temperature at the SEN wall started to drop below the liquidus. With the progress of the clogging front, the temperature at the SEN wall dropped dramatically, indicating that the clog promotes solidification. In **Figure 4b**, profiles of velocity ( $|\vec{u}|$ ), turbulence kinetic energy ( $k$ ), and specific dissipation rate ( $\omega$ ) are shown along the radius of the SEN when the clog thickness is 6 mm. It shows that in the clogging region, i.e., distance smaller than 6 mm, velocity is very small and turbulence is negligible.

The modeling result of the solidification along the SEN wall is shown in **Figure 5**. The evolution of the as-solidified region is presented in terms of the liquidus and solidus isosurfaces, and their average distances (data points) from the SEN wall

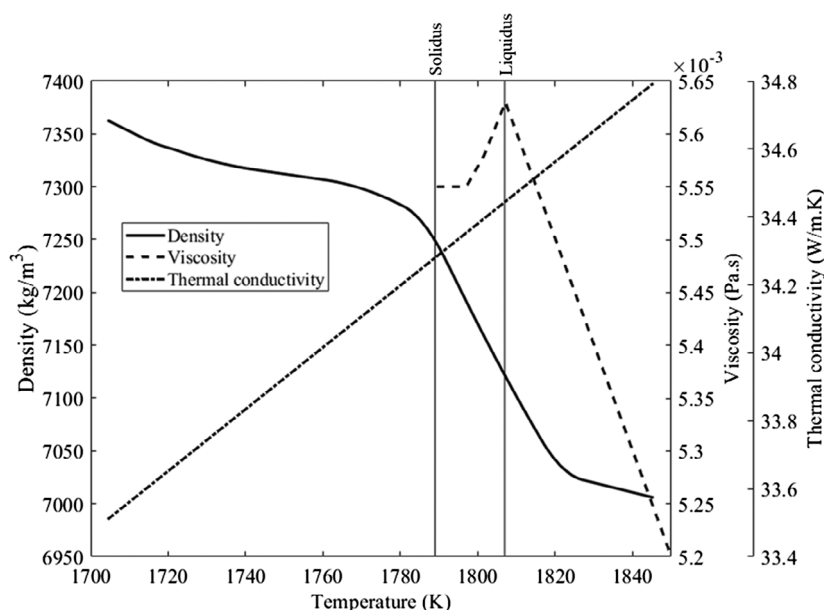


**Figure 3.** Density, viscosity, and thermal conductivity of steel as functions of temperature. The liquidus and solidus temperatures are shown with vertical lines. Data are taken from the IDS (InterDendritic Solidification) software<sup>[23]</sup> assuming that the steel composition corresponds to low-carbon steel (0.05 wt% C).



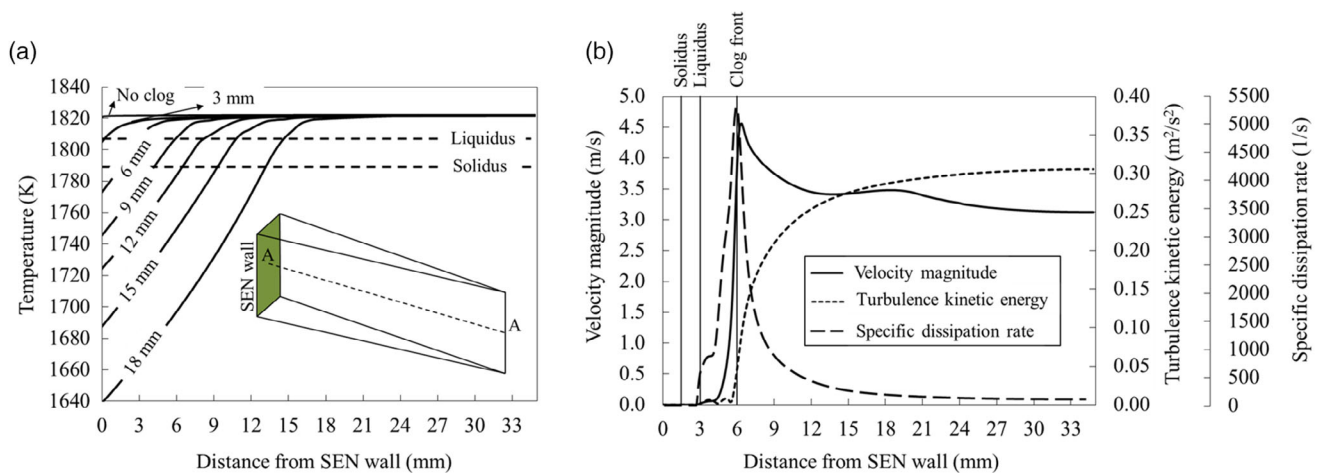


**Figure 4.** a) Influence of clog growth on the temperature profile and b) profiles of flow variables for clog thickness of 6 mm along line AA in the middle of the last calculation section (35). Here, the thermal conductivity of the SEN refractory is  $18.0 \text{ W m}^{-1} \text{ K}^{-1}$ .

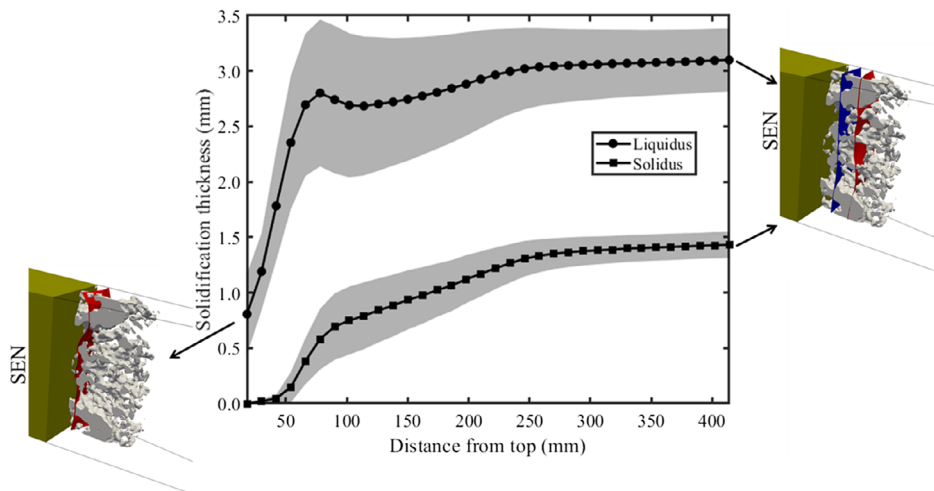


**Figure 5.** Solidification profile along the SEN wall in the vertical direction as the clog grows to 6 mm. The solidus and liquidus isosurface positions (distances from the SEN wall) are plotted. The data points show the averaged liquidus and solidus positions, whereas the gray areas portray the standard deviation. Here, the thermal conductivity of the SEN is  $18.0 \text{ W m}^{-1} \text{ K}^{-1}$ .

are presented. The gray areas indicate the standard deviation. Here, as a model assumption, the clog thickness is constant for the whole length along the SEN. Representatively, the solidus (blue) and liquidus (red) isosurfaces, together with the porous structure of the clog, are shown for the very first and last sections. In the first section, the temperature in the clog region is so high that the solidus isosurface does not appear.

In the upper part of the SEN, the thickness of the as-solidified region increased with the distance from the SEN top. In the lower part, the thickness became almost constant at distances larger than 300 mm from the SEN top. Similarly, the standard deviation of the isosurface position decreased with the distance from the SEN top. The solidus and liquidus isosurfaces became flatter, i.e., the solidification stabilized in the lower part of the SEN.

**Figure 6** shows the clog growth and its effect on the melt flow and solidification. The two isosurfaces, solidus (blue) and liquidus (red), divide the calculation domain into three regions:

solid steel (behind the solidus), mushy zone, and liquid steel (in front of the liquidus). The streamlines illustrate the flow field. As the melt mass flow rate across the whole SEN section was kept constant and the inner flow area decreased with the clog growth, the velocity magnitude of flow increased. The flow streamlines in the bulk of the SEN were vertical and parallel. Inside the clog region, the melt penetrated and flowed through the open pores/channels in the clog structure. In the solidification mushy zone, the flow was still visible but very weak.

Detailed information on solidification and flow field inside the clog is shown in **Figure 7** on a vertical surface when clog thickness is 6 mm. Due to the steady-state simulation, the temperature of steel and clog is identical. Inside the clog, flow is very slow and turbulence is damped. Turbulence is high on the clog front where the bulk flow meets the rough clog front.

To study the influence of the SEN refractory material on the solidification during clogging, a numerical parameter study was

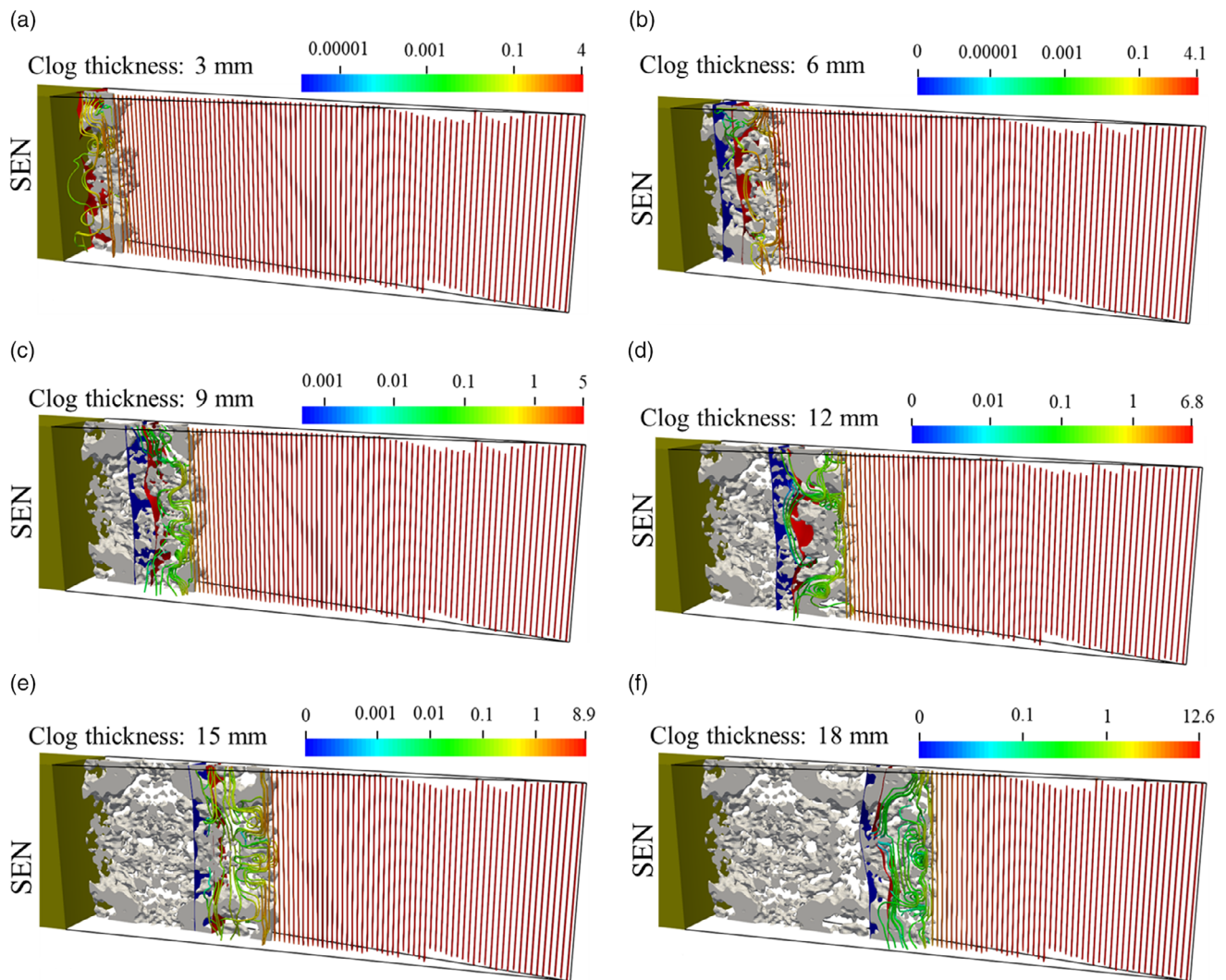


**Figure 6.** Solidification process in response to the clog growth. a–f) The clog thickness is 3, 6, 9, 12, 15, and 18 mm. The modeling results are presented for only the last section (35). The solidification regions are indicated by the solidus (blue) and liquidus (red) isosurfaces. The flow field is denoted by streamlines, and the velocity magnitude [ $\text{m s}^{-1}$ ] is shown in color scale. For better visualization, the results for only half of the calculation domain are shown. Here, the thermal conductivity of the SEN is  $18.0 \text{ W m}^{-1} \text{ K}^{-1}$ .

performed by varying the material's thermal conductivity ( $\lambda_{\text{SEN}}$ ) values. **Figure 8a** shows the thickness of the as-solidified region as a function of the clog thickness for the three SEN materials with  $\lambda_{\text{SEN}} = 6.0, 11.0, \text{ and } 18.0 \text{ W m}^{-1} \text{ K}^{-1}$ . In all the cases, the thickness of the as-solidified region increased with the clog. The smaller the thermal conductivity, i.e., more isolating the SEN refractory material, the thinner the as-solidified region. In **Figure 8a**, a dotted line is plotted representing the position of the clog front. By evaluating the distance between the clog front and the solidification front (isosurface; with  $f_s = 0.7$ ), a so-called open-channel clog thickness can be obtained. In the open-channel clog region, the flow was active and there was nil ( $f_s = 0.0$ ) or only partial solidification ( $0.0 \leq f_s < 0.7$ ). As shown in **Figure 8b**, during the clogging, the open-channel clog thickness was almost constant but strongly dependent on the SEN refractory material. The more isolating the SEN refractory material, the larger the open-channel clog thickness. The open-channel clog

thickness is believed to be an important parameter for the analysis of the clog stability, or the fragmentation and detachment, which is further discussed in following section.

## 4. Discussion

One of the concerns in the current model is its sensitivity to the computational cell size. To reproduce the clog structure with the best resolution, the cell size should be similar to or even smaller than the pixel size used in the original X-ray tomography ( $\approx 0.022 \text{ mm}$ ). In such a case, for the considered section in **Figure 1b**, the number of cells would have to be set at 54 million, which would increase the simulation time excessively. Therefore, a relatively coarse mesh with a cell size of  $0.12 \text{ mm}$  was used. This cell size seems reasonable, because it is fine enough to resolve the narrow channels ( $\approx 0.19 \text{ mm}$ ) of the clog structure, when the

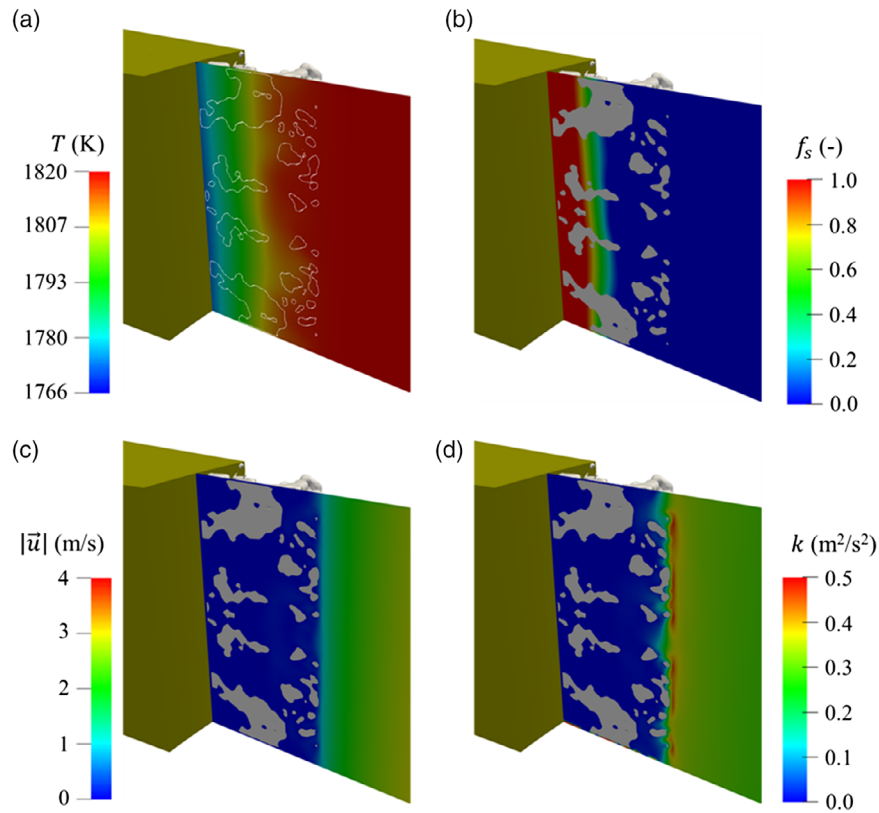


**Figure 7.** Calculated fields on a vertical surface when clog thickness is 6 mm: a) temperature, b) solid fraction, c) velocity magnitude, and d) turbulence kinetic energy. Here, the thermal conductivity of the SEN is  $18.0 \text{ W m}^{-1} \text{ K}^{-1}$ .

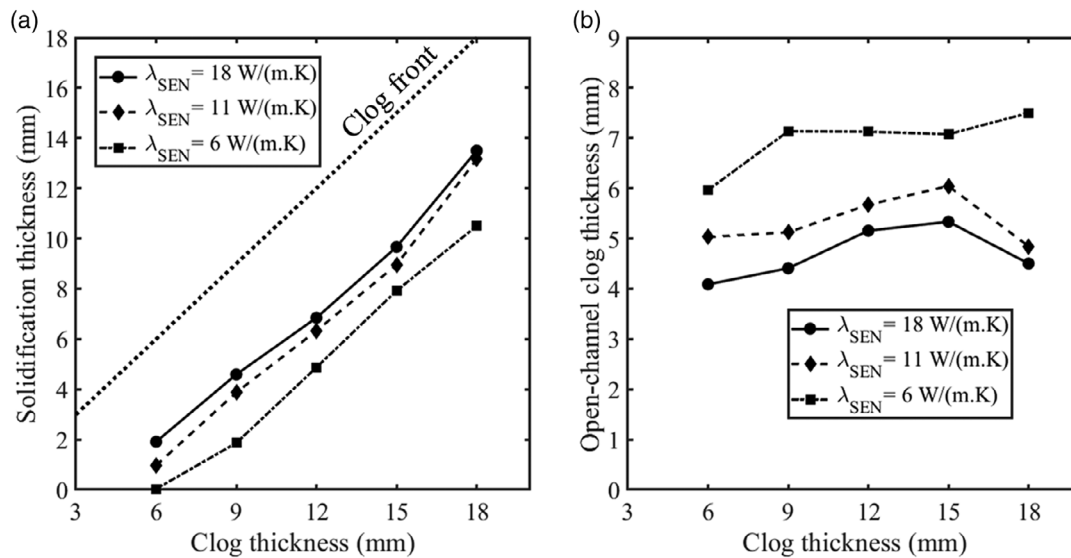


**Figure 8.** Influence of the SEN refractory material ( $\lambda_{\text{SEN}} = 6, 11, 18 \text{ W m}^{-1} \text{ K}^{-1}$ ) on the solidification during clogging. The thickness of the as-solidified region is defined as the distance between the SEN wall and the isosurface ( $f_s = 0.7$ ). a) The thickness of the as-solidified region as a function of clog thickness, where a dotted line is plotted as a reference for the clog front position; b) open-channel clog thickness, i.e., the distance between the clog front and the solidification front (isosurface with  $f_s = 0.7$ ).

number of cells is set as approximately 0.8 million. A comparison between the modeling results obtained using the finest mesh ( $\approx 0.022 \text{ mm}$ ) and the coarse mesh ( $\approx 0.12 \text{ mm}$ ) is shown in

**Figure 9.** The average temperature difference between these cases is only 0.032%, and the liquidus and solidus isosurface positions are also almost identical in both the cases. That means

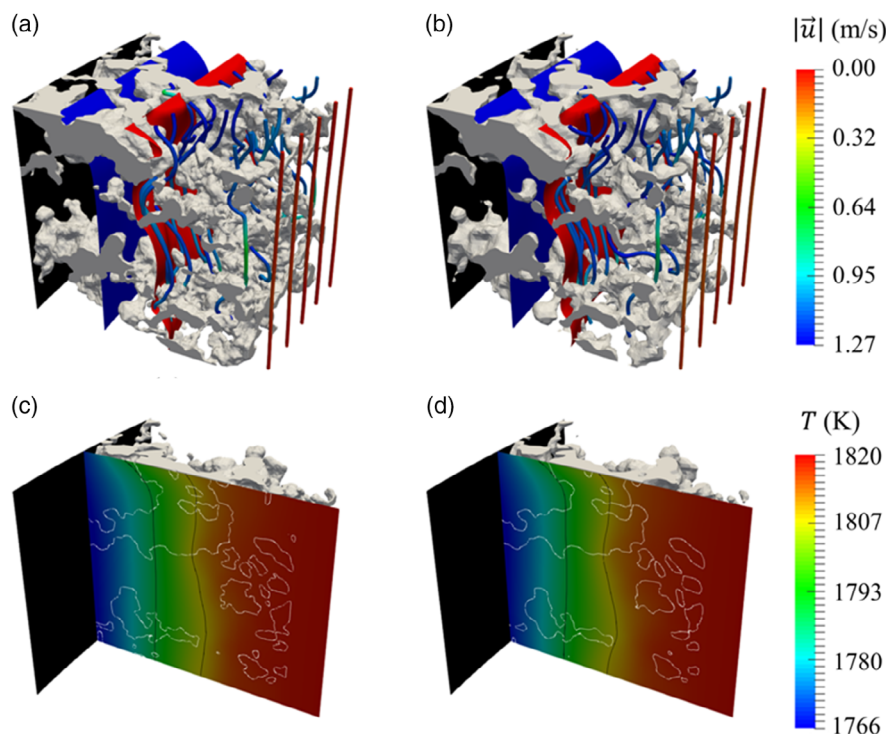


**Figure 9.** Comparison of modeling results using a) the finest mesh and b) the coarse mesh, where blue and red isosurfaces show the solidus and liquidus, respectively. The temperature fields on a vertical plane are also compared for c) the finest mesh and d) the coarse mesh; the white lines represent the clog structure on the selected cross-section and the black lines denote the solidus and liquidus. The black surface is the inner wall of the SEN.

solidification is not changed by mesh refining. Therefore, the cell size of 0.12 mm is fine enough to ensure the calculation accuracy of the solidification. The flow fields, illustrated by streamlines, are slightly different between the two cases. This difference seems ignorable for the solidification occurring in very deep clog regions.

It has been believed that the main mechanism for the occurrence of clogging is the gradual deposition of NMIs on the SEN wall and on the clog front.<sup>[11,13,14]</sup> A previous study on SEN clogging at the microscopic scale has shown that clogging is a highly transient and self-accelerating process, i.e., the clog growth rate increases with time.<sup>[18]</sup> The clogging process includes the initial coverage of the nozzle wall by the NMI particles, the evolution of a bulged clog front, and then the development of a branched structure. According to the self-accelerating nature of the clogging process, the time intervals for the development of the same clog thickness in Figure 6 should not be equal. The assumption of uniform clog thickness along the SEN wall might not be valid, especially in the late stages of the clogging when a large area of the SEN section is occupied by the clog. However, the focus of the current work is not to trace the growth kinetics of the clog, but to study the solidification, which occurs in response to the clog growth. The clog thickness along the SEN wall would never be uniform and, hence, the solidification behind the clog front would also be non-uniform, but the modeling results with respect to the solidification-clog relation should be valid, i.e., the calculated as-solidified shell thickness in response to the developing clog front should be valid.

In the current study, it was assumed that the clog structure is stable, rigid, and can withstand the drag force of the melt flow, and that there is no clog fragmentation. It is known that the

position of the stopper rod must be continuously adjusted (up and down) during the continuous casting process to compensate for the clog growth/fragmentation and to maintain a constant melt flow rate. This fact implies that the clogging and fragmentation occur alternatively. Occasionally, the clog structure itself may be very weak, even breakable with a finger touch. If the clog is reinforced by as-solidified steel, the clog region becomes stable.<sup>[10]</sup> According to the modeling results shown in Figure 8b, only the open-channel clog region, where there is no solid steel, may be sensitive to fragmentation and more prone to detachment due to the impact of the melt flow. Hypothetically, the numerically calculated open-channel clog thickness may serve as an indicator for the development of clog fragmentation. The critical thickness required for the open-channel clog region to withstand the drag force of the melt flow may depend on the clog mechanical strength, the clog chemical composite (e.g.,  $\text{Al}_2\text{O}_3$ ), the clog morphology, or even the cast steel grade. However, further study is required to verify this hypothesis.

The current modeling result (Figure 8) demonstrates that an SEN with thermally conductive refractory material is prone to solidification, and solidification helps stabilize the clog structure. Conversely, it can be expected that an isolating refractory material may extend the service life of the SEN, because of the large thickness of the open-channel clog region and its susceptibility to fragmentation. This is similar to the case when a well-preheated SEN is used. The use of the isolating-material SEN and the well-preheated SEN postpones the solidification of steel within the clog structure. It was observed in a steel plant that a SEN treated with enhanced preheating favored delayed clogging.<sup>[9]</sup>



The current numerical study is based on only one clog structure, shown in Figure 1a. The key features of the clog structure that influence the solidification are its porosity, size, and volume fraction of the open pores/channels. The exact mechanism through which the clog structure and its features depend on the alloy/process conditions, such as the cast steel grades, pre-treatment of the melt, and the type and amount of NMIs is still not clear. A study of the clog structure and its dependency on the steel grade and other process conditions would be an interesting subject for future research. Moreover, a study of the mechanical strength of the clog structure, which withstands the impact of the melt flow (and prevents fragmentation), would be another interesting subject. Clog growth and fragmentation are two sides of the same process and exert mutual balance. According to the modeling results shown in Figure 6–8, the clog structure must have sufficient mechanical strength to withstand the melt flow before it is stabilized by solidification. If the mechanical strength of the clog structure is too low (prone to fragmentation), an open-channel region with sufficient thickness will never develop before the solidification occurs. Again, the mechanical strength of the clog would depend on the alloy/process conditions as well.

## 5. Conclusions

An enthalpy-based mixture continuum model was used to study solidification in an as-clogged structure of an SEN during continuous casting of steel. This study contributes to the literature by clarifying a confusing point in a debate on the role of solidification in SEN clogging: whether the SEN clogging originates from the solidification, or does the clogging cause the solidification. The main conclusions of the study are as follows: 1) Solidification cannot occur before clogging if the molten steel has sufficient superheat (e.g., 20 K) and the SEN is properly preheated. Solidification plays a role in stabilizing/strengthening the clog structure. This statement supports a previous study by the current authors.<sup>[17]</sup> 2) Solidification occurs deep in the porous network of the clog structure as the melt flow stops. A so-called open-channel clog region exists in front of the solidification front, and has to be mechanically strong enough to withstand the impact of the melt flow; otherwise, the clog undergoes fragmentation. The calculated thickness of the open-channel clog region, depending on the clog structure (porosity, size, and volume fraction of the open pores/channels), can serve as an indicator of the fragmentation. 3) A SEN composed of an isolating refractory material can postpone the clogging and hence extend its service life.

## Acknowledgements

The authors gratefully acknowledge the funding support of K1-MET GmbH, metallurgical competence center. The research programme of the K1-MET competence center is supported by COMET (Competence Center for Excellent Technologies), the Austrian programme for competence centers. COMET is funded by the Federal Ministry for Climate Action, Environment, Energy, Mobility, Innovation and Technology, the Federal Ministry for Digital and Economic Affairs, the Federal States of Upper Austria, Tyrol and Styria as well as the Styrian Business Promotion Agency (SFG). In addition to the public funding from COMET, this research project is partially financed by the scientific partners (Montanuniversität Leoben and Johannes Kepler

University Linz) and the industrial partners (voestalpine Stahl Linz GmbH, voestalpine Stahl Donawitz GmbH, and RHI Magnesita GmbH). The authors also thank University of Applied Sciences Upper Austria for performing X-ray tomography of the as-clogged piece in SEN.

## Conflict of Interest

The authors declare no conflict of interest.

## Keywords

clogging, continuous castings, solidification, steel castings

Received: April 28, 2020

Revised: July 2, 2020

Published online: July 29, 2020

- [1] Y. Miki, H. Kitaoka, T. Sakuraya, T. Fujii, *ISIJ Int.* **1992**, 32, 142.
- [2] L. Zhang, B. G. Thomas, *Metall. Mater. Trans. B*, **2006**, 37, 733.
- [3] S. Basu, S. K. Choudhary, N. U. Girase, *ISIJ Int.* **2004**, 44, 1653.
- [4] Y. Vermeulen, B. Coletti, B. Blanpain, P. Wollants, J. Vleugels, *ISIJ Int.* **2002**, 42, 1234.
- [5] K. Sasai, Y. Mizukami, *ISIJ Int.* **1994**, 34, 802.
- [6] P. M. Benson, Q. K. Robinson, C. Dumazeau, in *Unitec'93 Congress*, Sao Paulo, Vol. 31, **1993**.
- [7] G. C. Duderstadt, R. K. Iyengar, J. M. Matesa, *JOM*, **1968**, 20, 89.
- [8] J. W. Farrell, D. C. Hilty, in *Electric Furnace Proc.*, Vol. 29, American Institute of Mining, Metallurgical, and Petroleum Engineers (AIME), New York **1971**, pp. 31–46.
- [9] S. Rödl, H. Schuster, S. Ekerot, G. Xia, N. Veneri, F. Ferro, S. Baragiola, P. Rossi, S. Fera, V. Colla, G. Bioli, M. Krings, L. F. Sancho, A. Diaz, M. Andersson, N. Kojola, *New Strategies for Clogging Prevention for Improved Productivity and Steel Quality*, Final Report, European Commission, Luxembourg **2012**.
- [10] K. G. Rackers, B. G. Thomas, in *78th Steelmaking Conf. Proc.*, Vol. 78, Iron and Steel Society, Warrendale **1995**, pp. 723–734.
- [11] B. G. Thomas, H. Bai, in *Steelmaking Conf. Proc.*, Vol. 84, Iron and Steel Society, Warrendale **2001**, pp. 895–912.
- [12] N. Kojola, S. Ekerot, P. Jönsson, *Ironmak. Steelmak.* **2011**, 38, 81.
- [13] N. Kojola, S. Ekerot, M. Andersson, P. G. Jönsson, *Ironmak. Steelmak.* **2011**, 38, 1.
- [14] Z. Deng, M. Zhu, B. Zhong, D. Sichen, *Metall. Mater. Trans. B* **2014**, 54, 2813.
- [15] D. Janis, A. Karasev, R. Inoue, P. G. Jönsson, *Steel Res. Int.* **2015**, 86, 1271.
- [16] Z. Deng, M. Zhu, Y. Zhou, D. Sichen, *Metall. Mater. Trans. B*, **2016**, 47, 2015.
- [17] H. Barati, M. Wu, A. Kharicha, A. Ludwig, *Solidification and Gravity VII* (Eds: G. K. A. Roósz, Zs. Veres, M. Svéda), Hungarian Academy of Sciences, Miskolc-Lillafüred **2018**, pp. 144–149.
- [18] H. Barati, M. Wu, A. Kharicha, A. Ludwig, *Powder Technol.* **2018**, 329, 181.
- [19] H. Barati, M. Wu, A. Kharicha, A. Ludwig, *Metall. Mater. Trans. B* **2019**, 50, 1428.
- [20] F. R. Menter, *AIAA J.* **1994**, 32, 1598.
- [21] J. P. Gu, C. Beckermann, *Metall. Mater. Trans. A* **1999**, 30, 1357.
- [22] Y. Tang, G. Hackl, G. Nitzl, S. P. A. Košir, in *STEELSIM 2017*.
- [23] J. Miettinen, S. Louhenkilpi, H. Kytönen, J. Laine, *Math. Comput. Simul.* **2010**, 80, 1536.